A straight quantum wave guide with mixed Dirichlet and Neumann boundary conditions in uniform magnetic fields

2007 J. Phys. A: Math. Theor. 40 4609

(http://iopscience.iop.org/1751-8121/40/17/014)

IOP Publishing Journal of Physics A: Mathematical and Theoretical

J. Phys. A: Math. Theor. **40** (2007) 4609–4633 doi:10.1088/1751-8113/40/17/014

A straight quantum wave guide with mixed Dirichlet and Neumann boundary conditions in uniform magnetic fields

O Olendski[1,3] **and L Mikhailovska**[2]

[1] Atomic and Molecular Engineering Laboratory, Belarusian State University, Skarina Avenue 4, Minsk 220050, Belarus
[2] Department of Higher Mathematics, Military Academy, Minsk 220057, Belarus

E-mail: oleg.olendski@jsums.edu

Received 3 January 2007, in final form 19 February 2007
Published 11 April 2007
Online at stacks.iop.org/JPhysA/40/4609

Abstract

A straight quasi-one-dimensional Dirichlet wave guide with a Neumann window of length L on one or two confining surfaces is considered theoretically with and without perpendicular homogeneous magnetic field **B**. It is shown that for the field-free case, a bound state in the continuum (BIC) for one Neumann window exists for some critical lengths only, while for the two Neumann segments symmetrically located on the opposite walls, due to the restored transverse symmetry of the system, BICs exist for the arbitrary L. Bound states lying below the fundamental propagation threshold of the Dirichlet strip survive any strength of the uniform magnetic field and do not depend on its direction. Moreover, an increasing field induces new bound states regularly arranged with the levels present at $B = 0$. For two Neumann windows, strong magnetic fields lead to the degeneracy of the adjacent odd and even bound states with their energies almost equal to each other and to their corresponding counterpart for one Neumann segment, which is explained by mapping the problem onto the field-free one or two purely attractive one-dimensional quantum wells with field-dependent depth. Miscellaneous magnetotransport characteristics of the structures are also considered; in particular, it is demonstrated that small fields applied to the channel with two Neumann windows destroy BICs by coupling them to the continuum states. This is manifested in the conductance-Fermi energy dependence by Fano resonances. Currents flowing in the wave guide are investigated too, and it is shown that current density patterns near the resonances form vortices which change their chirality as energy sweeps through the resonant region. Generalizations to any other arbitrary combination of the boundary conditions are provided. Comparison with other structures such as window-coupled Dirichlet wave guides, a bent strip or straight Dirichlet channel with electrostatic impurity inside, is performed.

[3] Present address: Department of Physics, Jackson State University, Jackson, MS 39217 USA.

PACS numbers: 03.65.Ge, 03.65.Nk, 75.47.−m, 73.63.−b

(Some figures in this article are in colour only in the electronic version)

1. Introduction

Interest in the properties of quantum wave guides has been steadily increasing after the experimental discovery of the conductance quantization in these ultra-small manmade structures [1, 2]. For example, theoreticians thoroughly discussed transport and electronic properties of semiconductor wave guides when an electrostatic scatterer [3–12] distorts laminar charge flow in the straight duct. In particular, it was shown that an asymmetrically embedded into the straight wave guide attractive impurity leads to the Fano resonances [13] on the conductance versus Fermi energy dependence. Apparently, these resonances were observed experimentally [14]. From a mathematical point of view, semiconductor quantum wave guides obey Dirichlet boundary condition of vanishing wavefunction $\Psi(\mathbf{r})$ at the external surfaces $\mathcal{L}$ of the nanostructure:

$$\Psi|_{\mathcal{L}} = 0. \tag{1}$$

However, wave guide systems are possible with combined Dirichlet and Neumann requirements. For the Neumann boundary condition a normal derivative of Ψ vanishes at the confining walls

$$\left.\frac{\partial \Psi}{\partial n}\right|_{\mathcal{L}} = 0, \tag{2}$$

with $\mathbf{n}$ being a unit vector perpendicular to the interface. Such systems can be formed, for example, by a superconductor sandwiched between normal metal and dielectric [15]. Properties of the wave guides with miscellaneous combination of different boundary conditions were theoretically addressed recently [16–20]. In particular, it was shown that an introduction of the Neumann window on one of the walls of the otherwise perfect Dirichlet straight channel leads to the existence of the bound state below the fundamental propagation threshold of the wave guide [16]. In a sense, introduction of the other type of the boundary condition presents a perturbation to the particle motion. However, this perturbation, instead of being caused by the explicit potential profile change between the plates as discussed above, is due to the variation of the confining walls. Below, we shall thoroughly discuss similarities and differences between these two situations. Setup with the Neumann window can be implemented, for example, by considering two straight semiconductor wave guides coupled laterally through the window [21, 22]. Recently, properties of the similar systems were intensively calculated [21–27]. It was shown, in particular, that for the small window lengths L the bound state below the fundamental propagation threshold appears from the continuum as the fourth power of L [25].

On the other hand, experimental discovery of the quantum Hall effect has spurred intensive theoretical and experimental research on magnetic field influence on low-dimensional nanostructures (see [28] and references therein). Properties of the straight semiconductor wave guides with scatterer in the perpendicular homogeneous magnetic fields were calculated [11, 29–37], and it was shown that applied field modifies drastically transmission spectra of the channel leading, for example, for some defect shapes, to the new resonances absent in zero field. Theoretical predictions of the new dips and peaks in the magnetic field were corroborated by the corresponding experiments [35, 38].

In the present paper, we study theoretically a straight quantum channel with different boundary conditions subjected to the uniform perpendicular magnetic field. To our knowledge, the problem of magnetic field influence on similar structures received almost no attention so far. In fact, the only known to us published result is stressed in [39] where it is proved theoretically that a bounded compactly supported field or the Aharonov–Bohm whisker can wipe out bound states lying below the fundamental propagation threshold of the straight Dirichlet wave guide with the Neumann window on one of the walls. Let us note that window-coupled in-plane-gated GaAs/$Al_xGa_{1-x}As$ wire systems were fabricated by means of modern technology, and their magnetotransport characteristics were measured showing, among other features, fine oscillatory patterns in the four-terminal resistance [40]. In contrast to these structures, for the systems we consider in the present paper, only two-probe measurements are relevant. This makes a substantial difference with coupled wave guides system since in the latter case zero derivative of the wavefunction is a simple consequence of the open boundary condition and in the former situation the Neumann condition is of the primary importance. As was stressed in [39], a Neumann window on the Dirichlet strip is a stronger perturbation to the particle motion than a protrusion [16, 21] or the window coupling to the other wave guide [21]; for example, the existence of the bound state for the wave guide with bump implies that the localized level below the continuum Dirichlet spectrum exists for the wave guide with the Neumann window [16]. Therefore, an investigation of the wave guide with different boundary conditions presents an original interest. As will be shown below, this is especially true in the case of applied magnetic fields. We derive exact formal expression for the scattering matrix of the wave guide by matching analytical solutions in each part of the channel. The same procedure is implemented for finding a transcendental equation which determines bound states below the fundamental propagation threshold. For the field-free case, we prove the existence of the localized levels embedded in the continuum; in particular, it is shown that for the one window it takes place for some special segment lengths only, and for the two Neumann windows on the opposite sides of the strip these states exist for arbitrary lengths. Magnetic fields destroy these levels by coupling them to their continuum counterparts what is manifested in the appearance of the Fano resonances on the conductance energy dependence. Another result of the application of the magnetic field is the field-induced bound states lying below the fundamental propagation threshold of the Dirichlet arms. Adjacent bound levels of the channel with two Neumann windows become degenerate at strong magnetic intensities what is explained by the one-dimensional model of coupled quantum wells with field-dependent profile. Currents flowing in the wave guide are also investigated, and their characteristic features such as formation and evolution of the vortices are discussed.

The paper is organized as follows. In section 2 our model is presented and a necessary formulation of our method is given. Several advantages of this approach are also discussed. Section 3 is devoted to the presentation and detailed physical interpretation of the calculated results. Summary of the results is provided in section 4. In the appendix we write the explicit form of the scattering and reflection matrices and the transcendental equation for bound state energies.

2. Model and formulation

Structure we consider is shown schematically in figure 1. Infinitely long straight quasi-one-dimensional (Q1D) wave guide of width d with the same type of the boundary conditions on both walls has on one (figure 1(a)) or two (figure 1(b)) confining surfaces a segment of length L where the boundary requirements are changed (say, from the Dirichlet to Neumann or vice versa). The whole system is subjected to the uniform magnetic field $\mathbf{B}$ pointing in the positive z

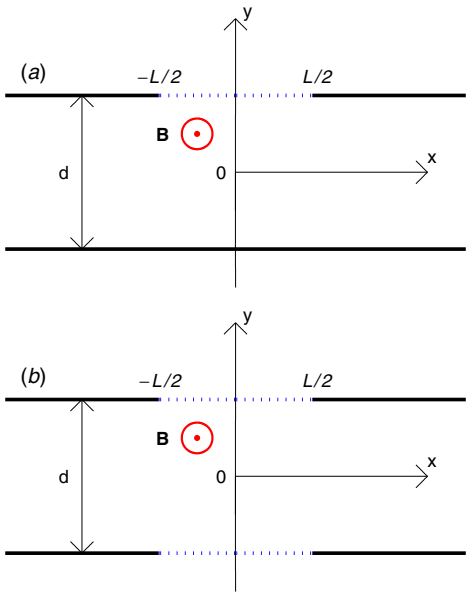

Figure 1. Straight wave guide of width d in homogeneous magnetic field $\mathbf{B}$ pointing in the positive z direction. Uniform boundary conditions for the semi infinite leads (thick solid lines) are interrupted by the segment of length L with the other type of boundary conditions on (a) one or (b) two confining walls (dotted lines). Cartesian coordinate system (x, y) is shown by thin solid lines. Its origin coincides with the middle of the corresponding junction.

direction. For brevity, we will denote each part of the wave guide by the two characters—either D for Dirichlet or N for Neumann—where the first (second) one corresponds to the boundary condition on the lower (upper) edge. Thus, figure 1(a) in our notation corresponds to a DD–DN–DD or NN–ND–NN structures, and figure 1(b)—to a DD–NN–DD or NN–DD–NN ducts.

For finding properties of the system, one needs to solve the Schrödinger equation for the wavefunction $\Psi(\mathbf{r})$

$$\left[\frac{1}{2M}(-\mathrm{i}\hbar\nabla + q\mathbf{A})^2 + V(\mathbf{r})\right]\Psi(\mathbf{r}) = E\Psi(\mathbf{r}). \tag{3}$$

Here M is a particle mass, q is an absolute value of its charge, and the confining potential $V(\mathbf{r})$ is zero inside the wave guide with its impenetrable walls effectively forbidding particle penetration outside of the duct

$$\Psi(x, |y| > d/2) \equiv 0. \tag{4}$$

Equation (3) may be used for the description of semiconductor nanostructures [41] within effective-mass approximation [42] as well as superconductors when the temperature T or/and magnetic field $\mathbf{B}$ are close to the material critical values T_c and B_c, respectively [15]. For the semiconductors M is equal to the effective mass m_e^* of the corresponding material, and $q = e$ with e being an absolute value of the electronic charge. For the superconductors $M = 2m_e$ with m_e being a bare electronic mass, and $q = 2e$. For both cases we neglect spin degrees of freedom. In addition, a magnetic field $\mathbf{B} = (0, 0, B)$ enters (3) via the vector potential $\mathbf{A}$, $\mathbf{B} = \nabla \times \mathbf{A}$.

It is convenient at this point to introduce dimensionless variables; namely, we will measure all distances in units of the wave guide width d; all energies, in units of ground-state energy $\pi^2\hbar^2/(2Md^2)$ of the infinite DD quantum well of width d; all momenta, in units of $\hbar/d$; magnetic fields, in units of $\hbar/(qd^2)$; time, in units of $2Md^2/(\pi^2\hbar)$; velocity, in units of $\hbar/(Md)$; conductance, in units of q^2/h; magnetic flux, in units of h/q; and two-dimensional current density, in units of $q\hbar/(Md^3)$.

For our problem we choose the vector potential $\mathbf{A}$ in the Landau gauge, $\mathbf{A} = (-yB, 0, 0)$. Then, in each part of the wave guide, general solution can be represented in the form where x and y variables are separated (below throughout the paper we disregard trivial z dependence):

$$\Psi(x, y) = \mathrm{e}^{\mathrm{i}px}\chi_p(y), \tag{5}$$

where function $\chi_p(y)$ satisfies the equation

$$\left(\frac{\mathrm{d}^2}{\mathrm{d}y^2} + [\pi^2 E - (By - p)^2]\right)\chi_p(y) = 0. \tag{6}$$

Equation (6) is accompanied by the boundary conditions on the confining walls; namely, for the DD case one has

$$\chi_p\left(\pm\tfrac{1}{2}\right) = 0; \tag{7}$$

for the DN configuration

$$\chi_p\left(-\frac{1}{2}\right) = 0, \tag{8a}$$

$$\left.\frac{\mathrm{d}\chi_p(y)}{\mathrm{d}y}\right|_{y=1/2} = 0; \tag{8b}$$

for the ND case

$$\left.\frac{\mathrm{d}\chi_p(y)}{\mathrm{d}y}\right|_{y=-1/2} = 0, \tag{9a}$$

$$\chi_p\left(\frac{1}{2}\right) = 0; \tag{9b}$$

and for the NN system

$$\left.\frac{\mathrm{d}\chi_p(y)}{\mathrm{d}y}\right|_{y=\pm 1/2} = 0. \tag{10}$$

Below, in order to prevent a confusion, we will write, if necessary, the function $\chi_p(y)$ and the coefficients p with the two-character superscript denoting corresponding type of the boundary conditions.

Detailed analysis of the solution of (6) for the DD case, equation (7), was given before [33, 36, 43, 44]. Therefore, here we concentrate on the comparative analysis of the remaining three configurations drawing analogies, if it is relevant, with the DD situation as well. Similar to it, we have found it convenient to present solutions in the analytical form, namely, for the NN case

$$\chi_{p_n}(y) = \gamma_{p_n}\left[U'\left(\frac{\pi^2}{2}\frac{E}{B}, \mathrm{i}(2B)^{1/2}\left(\frac{1}{2} + \frac{p_n}{B}\right)\right)U\left(\frac{\pi^2}{2}\frac{E}{B}, \mathrm{i}(2B)^{1/2}\left(y - \frac{p_n}{B}\right)\right)\right.$$
$$\left. + U'\left(\frac{\pi^2}{2}\frac{E}{B}, -\mathrm{i}(2B)^{1/2}\left(\frac{1}{2} + \frac{p_n}{B}\right)\right)U\left(\frac{\pi^2}{2}\frac{E}{B}, -\mathrm{i}(2B)^{1/2}\left(y - \frac{p_n}{B}\right)\right)\right], \tag{11}$$

and for the DN and ND systems

$$\chi_{p_n}(y)=\gamma_{p_n}\left[U\left(\frac{\pi^2}{2}\frac{E}{B},\pm\mathrm{i}(2B)^{1/2}\left(\frac{1}{2}\pm\frac{p_n}{B}\right)\right)U\left(\frac{\pi^2}{2}\frac{E}{B},\mathrm{i}(2B)^{1/2}\left(y-\frac{p_n}{B}\right)\right)\right.$$
$$\left.-U\left(\frac{\pi^2}{2}\frac{E}{B},\mp\mathrm{i}(2B)^{1/2}\left(\frac{1}{2}\pm\frac{p_n}{B}\right)\right)U\left(\frac{\pi^2}{2}\frac{E}{B},-\mathrm{i}(2B)^{1/2}\left(y-\frac{p_n}{B}\right)\right)\right] \tag{12}$$

with the upper (lower) sign in (12) corresponding to the DN (ND) situation. $U(a,\xi)$ in (11) and (12) is a Weber parabolic cylinder function [45], and a prime denotes its derivative with respect to the second argument. Clear analogy between these three and the DD [44] cases is seen. The unknown coefficients γ_{p_n} should be determined from the orthonormalization condition. From the fundamentals of the Sturm–Liouville analysis [46] it directly follows that this normalization condition is the same for all four cases:

$$\int_{-1/2}^{1/2}(p_n+p_{n'}-2By)\chi_{p_n}(y)\chi_{p_{n'}}(y)\,\mathrm{d}y=\delta_{nn'}, \tag{13}$$

$\delta_{nn'}$ is a Kronnecker symbol. Equation (13) was used before [33, 43, 44] for the DD case.

Allowed values of the coefficients p_n are to be found from the boundary conditions. A form of the solutions, equations (11) and (12), automatically zeroes the wavefunction (for the DN and ND cases) or its derivative (for the NN case) on one of the walls. Applying the corresponding requirement to the second side of the strip, one arrives at the transcendental equation for the determination of the allowed values of p. For the NN case one has

$$U'\left[\frac{\pi^2}{2}\frac{E}{B},-\mathrm{i}(2B)^{1/2}\left(\frac{1}{2}-\frac{p_n}{B}\right)\right]U'\left[\frac{\pi^2}{2}\frac{E}{B},-\mathrm{i}(2B)^{1/2}\left(\frac{1}{2}+\frac{p_n}{B}\right)\right]$$
$$-U'\left[\frac{\pi^2}{2}\frac{E}{B},\mathrm{i}(2B)^{1/2}\left(\frac{1}{2}-\frac{p_n}{B}\right)\right]U'\left[\frac{\pi^2}{2}\frac{E}{B},\mathrm{i}(2B)^{1/2}\left(\frac{1}{2}+\frac{p_n}{B}\right)\right]=0, \tag{14}$$

and for the DN and ND cases, we obtain

$$U\left[\frac{\pi^2}{2}\frac{E}{B},-\mathrm{i}(2B)^{1/2}\left(\frac{1}{2}\pm\frac{p_n}{B}\right)\right]U'\left[\frac{\pi^2}{2}\frac{E}{B},-\mathrm{i}(2B)^{1/2}\left(\frac{1}{2}\mp\frac{p_n}{B}\right)\right]$$
$$+U\left[\frac{\pi^2}{2}\frac{E}{B},\mathrm{i}(2B)^{1/2}\left(\frac{1}{2}\pm\frac{p_n}{B}\right)\right]U'\left[\frac{\pi^2}{2}\frac{E}{B},\mathrm{i}(2B)^{1/2}\left(\frac{1}{2}\mp\frac{p_n}{B}\right)\right]=0 \tag{15}$$

with the same convention for the signs as in (12). The left-hand sides of (14) and (15) are considered as functions of momentum p_n for fixed E and B. We again draw parallels with the DD case [44]; namely, equation (14), if stripped of the primes, turns into its DD counterpart, equation (6) in [44]. The same transparent is the similarity between the DN and ND cases, since the corresponding equations (15) transform into each other with the change of the sign of p_n. In turn, equation (14) for the NN channel remains invariant under the transformation $p\to-p$, as is the case for the DD strip [43, 44]. Asymmetry of equations (15) with respect to the axis $p=0$ for the DN and ND configurations in the magnetic fields is a consequence of the fact that non-uniform boundary conditions, in contrast to the DD and NN requirements, introduce a transverse asymmetry when the upward motion is not equivalent to the downward one. Since applied magnetic field mixes transverse and longitudinal motions of the charged particles, this asymmetry naturally enters into the wave vectors $p_n^{(DN)}$ and $p_n^{(ND)}$ in (15). Note also that if some particular p_n is a solution of either (14) or (15), then its complex conjugate p_n^* satisfies the corresponding equation too.

Putting in (14) and (15) the value of p_n equal to zero, one can determine the energies of the vanishing wave vector:

$$\left(U'\left[\frac{\pi^2}{2}\frac{E}{B}, \mathrm{i}\left(\frac{B}{2}\right)^{1/2}\right]\right)^2 - \left(U'\left[\frac{\pi^2}{2}\frac{E}{B}, -\mathrm{i}\left(\frac{B}{2}\right)^{1/2}\right]\right)^2 = 0, \tag{16}$$

for the NN case, and

$$U\left[\frac{\pi^2}{2}\frac{E}{B}, \mathrm{i}\left(\frac{B}{2}\right)^{1/2}\right] U'\left[\frac{\pi^2}{2}\frac{E}{B}, \mathrm{i}\left(\frac{B}{2}\right)^{1/2}\right] + U\left[\frac{\pi^2}{2}\frac{E}{B}, -\mathrm{i}\left(\frac{B}{2}\right)^{1/2}\right] U'\left[\frac{\pi^2}{2}\frac{E}{B}, -\mathrm{i}\left(\frac{B}{2}\right)^{1/2}\right] = 0, \tag{17}$$

for the different boundary conditions on the opposite sides of the strip. Utilizing properties of the Weber functions [45], one can show that for $B = 0$ solutions of (16) transform to $E = (n-1)^2$, $n = 1, 2, \ldots$, and those of (17)—to $E = (n-1/2)^2$, as would be expected. Along the same lines, it can be derived that for the strong magnetic fields these energies approach asymptotically the equidistant Landau spectrum $E = (2n-1)B/\pi^2$. In fact, these two limiting cases can be in a much simpler way deduced directly from (6) with the appropriate boundary conditions and $p = 0$. Also, equation (14), similar to the DD case [44], has a countably infinite set of solutions with a finite number of real and infinitely many purely imaginary wave vectors where the nth imaginary $p_n^{(NN)}$, for the large n, has an asymptotic form of $p_n^{(NN)} \simeq \mathrm{i}[\pi n + \mathrm{O}(1/n)]$ which is independent of the energy E and magnetic field B. In turn, a countably infinite set of solutions for the DN configuration (upper sign in (15)) contains a finite number of real and infinitely many complex wave vectors with their real components, for the large enough n, decreasing to zero and being proportional to B, and imaginary parts, in the same limit, being of the form $\mathrm{Im}\left[p_{2n,2n+1}^{(ND)}\right] \simeq \pm\left(\frac{\pi}{2} + \pi n\right) + \mathrm{O}(1/n)$. Mathematically, these properties follow from the asymptotic expansions of the Weber function [45]. In addition, as will be shown below, (14) has, for some values of E and B, a finite number of complex solutions, as is the case for the DD strip too [33, 36, 43, 44].

Figure 2 shows wave vectors $p^{(DN)}$ as a function of the energy E for $B = 10$. Complex states are conveniently numbered by the increasing magnitude of the imaginary parts of $p_n^{(DN)}$. On the increase of the energy, absolute values of the imaginary parts decrease and at some points turn to zero. We see that solutions of two equations—(17)—that can be written in the following explicit form: $p_n(E) = 0$, and of the equation

$$\left.\frac{\partial E}{\partial \mathrm{Im}(p_n)}\right|_{\partial^2 E/\partial[\mathrm{Im}(p_n)]^2 \neq 0} = 0, \tag{18}$$

which were identical for the field-free case, are not equivalent in the presence of magnetic fields. For example, for the first complex state from figure 2, equation (18) is satisfied at $E = 0.602$. At this point, two complex wave vectors turn into two positive ones and, accordingly, we have two states with nonzero p_n while in the absence of the field these wave vectors are zero. One of the wave vectors increases, and the other one rapidly decreases, reaches zero at the energy satisfying (17) (in particular, in the case of figure 2 this takes place at energy $E = 0.934$), and at higher energies the corresponding level transforms into the state carrying current in the opposite direction. The wave number of this level decreases on further increase of energy. Described procedure of transformation of the complex states into two levels with positive p_n and their subsequent evolution is the same for the states with higher magnitudes of $\mathrm{Im}(p_n)$. For example, a second pair of the complex levels transforms into two states with positive p_n at $E = 3.105$. As we already mentioned, discussed here asymmetry of the dispersion

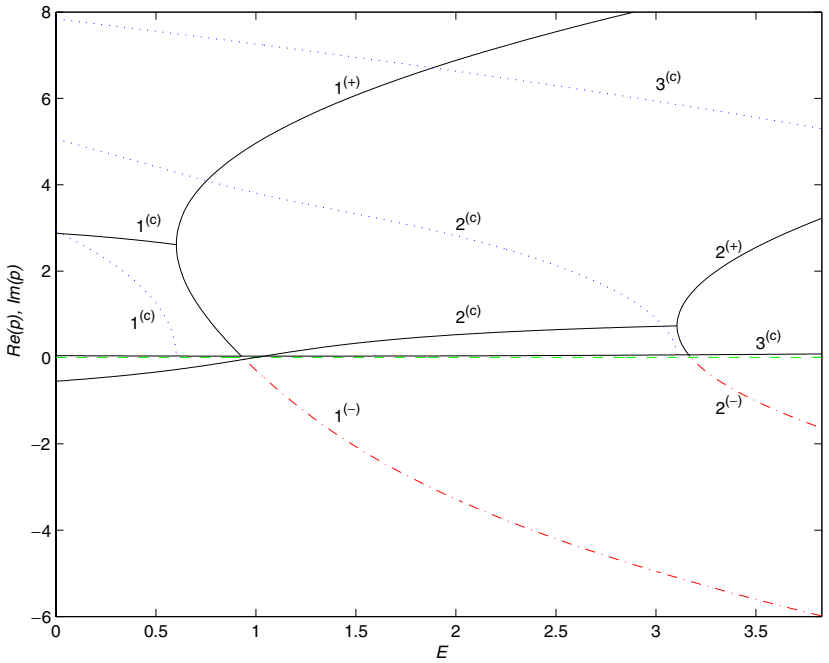

Figure 2. Propagation constants p_n of the DN wave guide as a function of the energy E for $B = 10$. States with positive (negative) p_n are plotted by the solid (dash-dotted) lines and denoted by the corresponding superscript near the level numbers. Real parts of the states with complex propagation constants are also shown by the solid lines and denoted by the superscript (c). Imaginary parts of the complex p_n are plotted by the dotted curves. Dashed line denotes the zero value of the wave vector.

relation of p_n is due to the nonequivalence of the up- and downward motions in the DN wave guide. The higher the field, the larger the asymmetry and, accordingly, the larger the difference between the solutions of (17) and (18). Comparing discussed here picture with the angular wave vector in the continuously curved DD wave guide [44], we see a complete qualitative analogy between these two situations since for the bent strip the magnetic field destroys angular symmetry too; namely, clockwise and counterclockwise motions are not equivalent, as they were at $B = 0$ [44].

Figure 3 shows positive real $\mathrm{Re}(p)$ and imaginary $\mathrm{Im}(p)$ components of the wave vector p in the NN wave guide as a function of the energy E for several magnetic fields B. As was stated above, the figure is symmetric with respect to the line $p = 0$. In the absence of the fields, a continuous spectrum of the NN strip starts at $E = 0$. Tiny magnetic fields lead to the small right shift of this fundamental propagation threshold and to the appearance of the new imaginary wave vector which, as figure 3(a) shows, lies below its counterparts present at $B = 0$. With growing magnetic field this level rapidly approaches higher lying wave vector, and when they stick together, their real components cease to be zero, acquiring values that are equal in magnitude and opposite in sign. The positive real part of the wave vector is shown in panels 3(b) and 3(c). Thus, instead of the evanescent motion, one has an oscillatory damped wave. With further growth of the energy, either real (panel 3(b)) or imaginary (panel 3(c)) component of these complex wave vectors turns to zero. As comparison of these two panels shows, for smaller fields the real part reaches zero first and, when this happens, imaginary

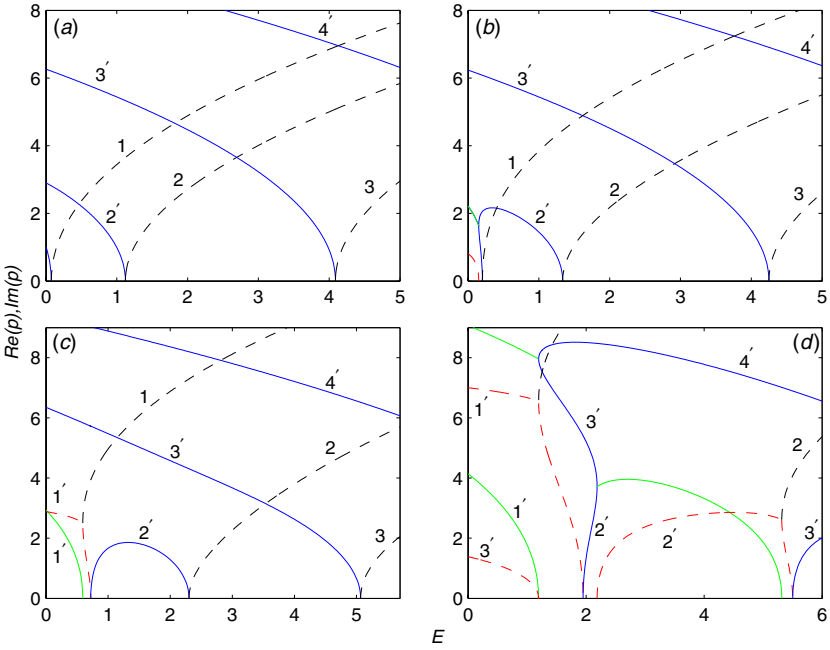

Figure 3. Momenta p_n of the straight NN channel in the magnetic field as a function of the energy E for several values of B: (a) $B = 3$, (b) $B = 5$, (c) $B = 10$ and (d) $B = 20$. Dashed lines are for the real part of the momentum, and the solid ones—for the imaginary constituents. Numbers near the propagating states denote the corresponding subbands, while primed numbers are used for the evanescent or oscillatory damped levels.

components of the wave vectors split off. One of them rapidly decreases and at the energy which is a lowest solution of (16), it transforms into the first propagating state. In turn, the higher lying imaginary wave vector becomes zero at the energy corresponding to the second solution of (16) when a new propagating channel opens up. In contrast to figure 3(b), for the higher magnetic fields the imaginary parts of $p_1^{(NN)}$ approach zero faster. In this case, as figures 3(c) and 3(d) show, their real components split off. One of them monotonically increases with E, and the second one decreases and at the lowest solution of (16) gives birth to the imaginary wave vector whose magnitude grows with energy, reaches maximum, decreases and turns to zero as the energy reaches a second solution of (16). At this point, second propagating channel emerges again. As comparison of figures 3(c) and 3(d) shows, the difference between the lowest solutions of the two equations—(16)—that can be written in the following explicit form: $p_n^{(NN)} = 0$, and of the equation

$$\left.\frac{\partial E}{\partial \mathrm{Re}(p_n)}\right|_{\partial^2 E/\partial[\mathrm{Re}(p_n)]^2 \neq 0} = 0, \tag{19}$$

increases with the field. Also, note that for stronger B (figure 3(d)) similar coalescences and splittings take place for the levels with larger magnitude in the fundamental propagation mode and for the wave vectors in higher subbands. Thus, dispersion of the NN channels possesses features both from the DD and DN strips; namely, similar to the DD case [44], the wave vector is symmetric with respect to $p = 0$; on the other hand, coalescences and splittings of the propagation constants resemble the corresponding picture for the DN wave guide.

Having learned the characteristic features of the wave dynamics for each type of the boundary conditions, one can construct solutions for the channel with their miscellaneous combinations. Consider, for example, the DD–DN–DD strip (figure 1(*a*)). A total solution to the left of the bend is

$$\Psi(x,y)=\sum_{n=1}^{\infty}\left[C_n\chi_{p_n}^{(DD)}(y)\exp\left(\mathrm{i}p_n^{(DD)}(x+L/2)\right)\right.$$
$$\left.+D_n\chi_{-p_n}^{(DD)}(y)\exp\left(-\mathrm{i}p_n^{(DD)}(x+L/2)\right)\right],\qquad x\leqslant -L/2. \tag{20}$$

The first sum in (20) describes the waves incident on the DN junction, with a second term being a set of reflected (for the real p_n) or localized near it (for the purely imaginary p_n) modes. Complex amplitudes C_n and D_n define the relative contribution of the nth subband into the total current.

Solution after the junction reads

$$\Psi(x,y)=\sum_{n=1}^{\infty}F_n\chi_{p_n}^{(DD)}(y)\exp\left[\mathrm{i}p_n^{(DD)}(x-L/2)\right],\qquad x\geqslant L/2. \tag{21}$$

Again, terms in (21) with real p_n describe the waves propagating away from the scatterer, while the terms with purely imaginary momenta are the states trapped by the DN part. For a particular case of C_n being a Kronnecker symbol, $C_n=\delta_{nm}$, $m=1,2,\ldots$, due to the flux conservation law the following relation holds for the energies E such that $E>E_{DDm}^{(TH)}$, with $E_{DDm}^{(TH)}$ being mth propagation threshold of the DD wave guide [44]:

$$\sum_{n=1}^{\infty}(|D_n|^2+|F_n|^2)\theta\left(E-E_{DDn}^{(TH)}\right)=1. \tag{22}$$

$\theta(x)$ in (22) is a step function, and terms $|F_n|^2$ and $|D_n|^2$ are, respectively, current transmission and reflection probabilities between the subbands m and n. It is necessary to note here that in the study of the scattering processes in the field-free Q1D channels, equation (22) usually contains an additional factor $v_n^{(DD)}/v_m^{(DD)}$ in the series of the left-hand side [4, 8]. Here $v_n^{(DD)}$ is a group velocity of the nth Dirichlet mode which in the general case of the nonzero B is written as

$$v_n^{(DD)}=p_n^{(DD)}-B\overline{y}_n, \tag{23}$$

with $\overline{y}_n$ being a centre of gravity of the same subband:

$$\overline{y}_n=\int_{-1/2}^{1/2}y\left|\chi_{p_n}^{(DD)}(y)\right|^2\mathrm{d}y. \tag{24}$$

However, in our treatment, as (13) shows, this group velocity is already included into the normalization condition which means that the wavefunctions $\chi_{p_n}(y)$ are normalized to the unit probability flux [43]. As a result, the velocity factor drops out from (22) [43].

In the DN junction, a total solution of (3) is

$$\Psi(x,y)=\sum_{n=1}^{\infty}Q_n\chi_{p_n}^{(DN)}(y)\exp\left(\mathrm{i}p_n^{(DN)}x\right),\qquad -L/2\leqslant x\leqslant L/2 \tag{25}$$

with index n running over all DN states discussed above.

Transport properties of the structure in the ballistic regime are completely determined by the scattering matrix $\mathbf{S}(E)$, which relates amplitudes of the incoming and transmitted waves in each subband. In our notation, it is

$$\mathbf{F}=\mathbf{SC}, \tag{26}$$

where amplitudes C_n and F_n from (20) and (21) form infinite column vectors $\mathbf{C}$ and $\mathbf{F}$, respectively. Matrix $\mathbf{S}(E)$ is a function of the Fermi energy E. It also depends on the parameter L. Knowledge of $\mathbf{S}(E)$ allows one to calculate the two-probe conductance [47]:

$$G(E) = \sum_{nn'} S^*_{nn'} S_{nn'}, \tag{27}$$

where the scattering matrix element $S_{nn'}$ defines the probability of the particle scattering from channel n to n' with the corresponding change of the group velocity. The sum in (27) runs over all open channels. Similar to (22), due to the normalization adopted in (13), the ratio $v^{(DD)}_{n'}/v^{(DD)}_{n}$, present in other studies [4, 9], is dropped out from the right-hand side of (27). For finding the scattering matrix, one needs to match solutions in the different regions at the junctions between them. This procedure leads to the expression for $\mathbf{S}$ whose explicit form is provided in the appendix. In the same way, one can calculate the reflection matrix $\mathbf{R}(E)$ linking amplitudes of incoming and reflected waves in different subbands,

$$\mathbf{D} = \mathbf{RC}. \tag{28}$$

Explicit expression for $\mathbf{R}$ is also provided in the appendix. Since the total energy of the system remains the same and incident, transmitted and reflected waves for each subband in (20) and (21) have the same normalization given by (13), it is easy to obtain from (26) and (28) that

$$\mathbf{S}^\dagger\mathbf{S} + \mathbf{R}^\dagger\mathbf{R} = \mathbf{I}, \tag{29}$$

with $\mathbf{I}$ being the unitary matrix. Equation (29) represents a general property of the unitarity of the scattering process [48] described, in our particular case, by the transmitted $\mathbf{S}$ and the reflected $\mathbf{R}$ matrices. In fact, equation (22) is another form of (29).

When one considers bound states lying below the fundamental propagation threshold of the DD arm, it is necessary to put all coefficients C_n in (20) equal to zero, $C_n \equiv 0$. The procedure of matching is completely similar to the one used for the scattering case, and leads then to the infinite linear algebraic system. Requirement of the vanishing of its determinant defines energies of the bound levels. The corresponding equation is written in the appendix. An infinite set of eigenvectors corresponding to the eigenenergies defines the coefficients D_n, F_n and Q_n. In other words, one can fully construct bound-state wavefunction in the magnetic field.

3. Results and discussion

3.1. Bound states

Without the field, bound states behaviour as a function of the length L is the same as for the coupled wave guides [21, 26, 27]; namely, their energies monotonically decrease with growing L and at large window lengths tend asymptotically to $1/4$ (for the DN inner part) or zero (for the NN junction). In turn, a number of the bound states increases with L [21, 26]. Note that the bound states (except the first one) for the NN part emerge from the continuum at the smaller lengths L, and their energies are always smaller than for the DN junction what can be explained by the stronger perturbation to the particle motion by the pure Neumann junction.

Next, we turn on the uniform magnetic field $\mathbf{B}$ and discuss bound states behaviour. Figure 4 shows their energies as a function of B for the DN and NN junctions and several lengths L. For comparison, a DD fundamental threshold that is a lowest solution of the prime-free equation (16) [44] is also shown. Since the bound states do not depend on the positive or negative z-direction of the field, only a case with $B \geqslant 0$ is depicted. It is seen that present at $B = 0$ bound states survive any strength of the homogeneous field. This is in a sharp

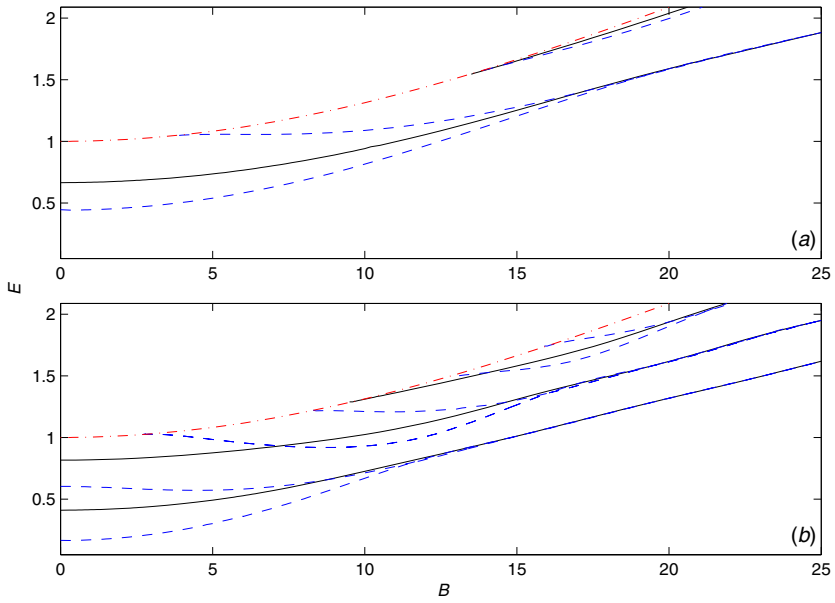

Figure 4. Bound state energies of the DD wave guide with DN (solid line) and NN (dashed line) junction as a function of the applied magnetic field B for the junction length (a) $L = 1$ (when one bound state exists at $B = 0$ for both configurations) and (b) $L = 2$ (with two bound states in vanishing fields for each case). Fundamental propagation threshold for the DD arms (least solution of equation (7) in [44]) is shown by the dash-dotted line.

contrast with a bounded compactly supported field which can empty the discrete spectrum of the DD–DN–DD wave guide [39]. Moreover, in our case new localized levels are formed with the growth of the uniform field B. A number of these magnetic-field-induced states increase with B. For the inhomogeneous fields vanishing at infinity, the problem was mapped onto the field-free superposition of the one-dimensional purely attractive square quantum well of width L and a field-dependent positive potential [39]. Such a system, for small enough L, has no bound state. In the spirit of [39], we can say that in the uniform magnetic field the problem of the Neumann window in the DD wave guide reduces to the one-dimensional quantum well whose depth increases with B, since it is known that a number of the localized levels in the quantum well grows with its depth [31]. Evolution of the number of the bound states below the continuous spectrum in open bounded simply or multiply connected two-dimensional domains in the miscellaneous non-uniform magnetic fields has been studied recently by several authors [49–51].

Bound states for the NN junction become degenerate for the strong fields. As figure 4 shows, with B growing, they couple into pairs with energies in each pair coming more and more closely to each other. For the increasing fields, these energies also coincide with the energy of the DN level which, in the absence of the fields, lay between them. Field-induced states undergo similar arrangement. In terms of [39], it means that for the NN junction we have two coupled field-free one-dimensional quantum wells with their depth growing with the field. Thus, for strong enough B, low-lying levels of such system become almost degenerate due to the strong suppression of the tunnelling between the wells with their energies practically indistinguishable and equal to their counterpart of the single quantum well. From basic principles of the wave dynamics [52], it is known that the state with the lower energy has a

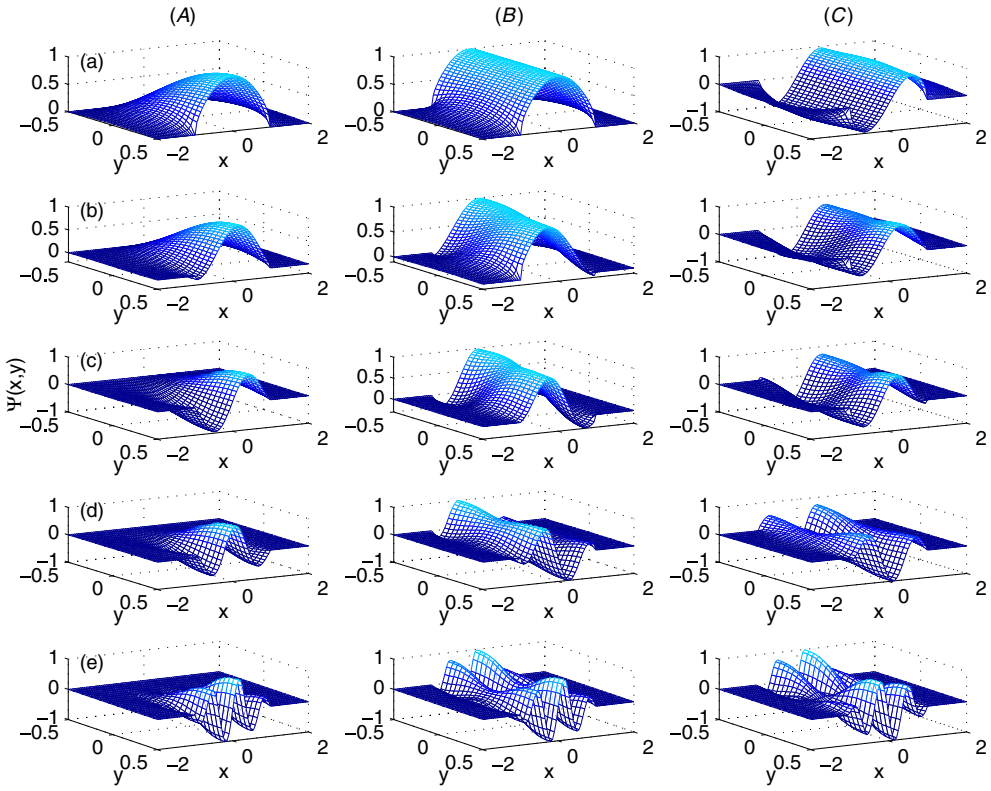

Figure 5. Wavefunction $\Psi(x, y)$ (normalized to its maximum) for the ground state of the wave guide with the DN junction (vertical column (A)), for the ground (column (B)) and first excited (column (C)) states for the NN inner part with $L = 2$ and several magnetic fields where horizontal row (a) is for $B = 0$, row (b) corresponds to $B = 6$, (c) $B = 10$, (d) $B = 15$, (e) $B = 25$.

symmetric wavefunction, and the higher level is an antisymmetric one. As we shall see, this is also the case for the DD–NN–DD wave guide in the uniform magnetic field.

Here, once again we draw parallels with the bent Dirichlet channel. Similar to the straight DD–DN–DD wave guide, it was proved theoretically that a bounded compactly supported field or the Aharonov–Bohm whisker can delete the bound state lying below the fundamental propagation threshold of the bent Dirichlet duct [53]. However, similar to our case, this level, that is formed as a result of the bend, survives arbitrary homogeneous fields [44]. A drastic difference between these two cases is in the asymptotic behaviour of the corresponding states at strong magnetic intensities. Namely, as B goes to infinity, the bound state of the curved [44] or crossed [43] Dirichlet channel transforms into the Landau level with influence of the wave guide boundaries monotonically decreasing on the strong magnetic background. In contrast, for the straight strip with the DN or NN part the Neumann sectors continue to play the decisive role in the formation of the bound states. In fact, with increasing magnetic field the Neumann segments attract particle more and more strongly. This is clearly seen in figure 5 that shows bound-state wavefunctions for the ground DN (vertical column (A)) and ground (column (B)) and first excited NN (column (C)) localized levels for $L = 2$ and several magnetic fields. Small and moderate **B** (horizontal panels (b) and (c) in figure 5) destroy symmetries which exist for the field-free wavefunctions (panel (a)). Strong magnetic fields push particle more

and more closely to the Neumann segment, simultaneously forming inside it the longitudinal oscillations of its wavefunction, as column (A) shows. For the DD–NN–DD duct an increasing magnetic intensity, while splitting the charge distribution between the Neumann parts on the opposite surfaces, at the same time creates a new symmetry of the bound states. As panels (e) of the columns (B) and (C) show, ground-state wavefunction becomes again transversely symmetric, and for the first excited state its wavefunction distribution is antisymmetric with respect to the middle line $y = 0$ of the strip. For $y > 0$, both these wavefunctions coincide (up to their sign) with their DN counterpart. Such a picture is in a complete accordance with the single (DN case) or two coupled (NN junction) one-dimensional quantum wells analogy described in two previous paragraphs. Namely, as the coupling between the wells diminishes what in our model corresponds to the increasing field, the ground-state energy of the quantum well approaches the higher lying level with their wavefunctions being, respectively, symmetric and antisymmetric ones. Since for the Neumann requirement a strong magnetic field is not the only determining factor, bound-state energies do not tend to the Landau levels at $B \to \infty$ increasing instead much slower, as figure 4 shows. Our discussion also enlightens the limited scope of the analogy between the DD channel with the DN or NN junction and the window-coupled wave guides picture. This correspondence, which might be valid at zero fields, breaks down at $B \neq 0$. For coupled wave guides the requirement of the vanishing $\partial\Psi/\partial y$ is of a secondary importance since it appears as a simple consequence of the coupling of the two Dirichlet wave guides (open boundary condition). However, for the DN junction the same requirement plays its independent and very significant role what is clearly seen for the nonzero fields.

3.2. Charge transport

3.2.1. Field-free case. Before addressing magnetotransport properties, it is instructive to investigate the processes taking place at zero fields. For $B = 0$, the corresponding wavefunctions transform into the linear combination of the products of the trigonometric and exponential functions. Since this form is well known [21, 26], we do not write it here.

Figure 6(a) shows conductance G as a function of the Fermi energy E for the DD–DN–DD channel and several L. In the fundamental mode, for very small window lengths, the conductance is unity almost everywhere but the mode boundaries. Near the fundamental propagation threshold, the conductance rapidly grows with energy and very soon approaches values very close to unity (dotted line in figure 6(a)). Another remarkable feature is a steep antiresonance slightly below the upper boundary of the mode. Interference of the discrete level split off by the DN segment from the higher lying subband, with the continuum states of the lower DD mode, causes the conductance to drop abruptly, and for the fundamental propagation subband, to vanish at some energy $E_{\min}$, which is determined by the length L. Thus, at this point we have a complete interference blockade of the charged-particle transport. The resonance is characterized by the energy $E_{\min}$ where zero minimum of the conductance is achieved, and by its half-width Γ, which defines the lifetime τ of the quasi-bound state

$$\tau = \frac{1}{\Gamma}. \tag{30}$$

In fact, one can say that a quasi-bound state has a complex energy E_{qb}:

$$E_{\mathrm{qb}} = E_{\min} - \mathrm{i}\Gamma/2. \tag{31}$$

For the present situation, we define Γ as a difference between the energies at which the value of the conductance $G = G_{<}/2$ is achieved where $G_{<}$ is the lesser of the two maxima surrounding zero minimum at $E_{\min}$.

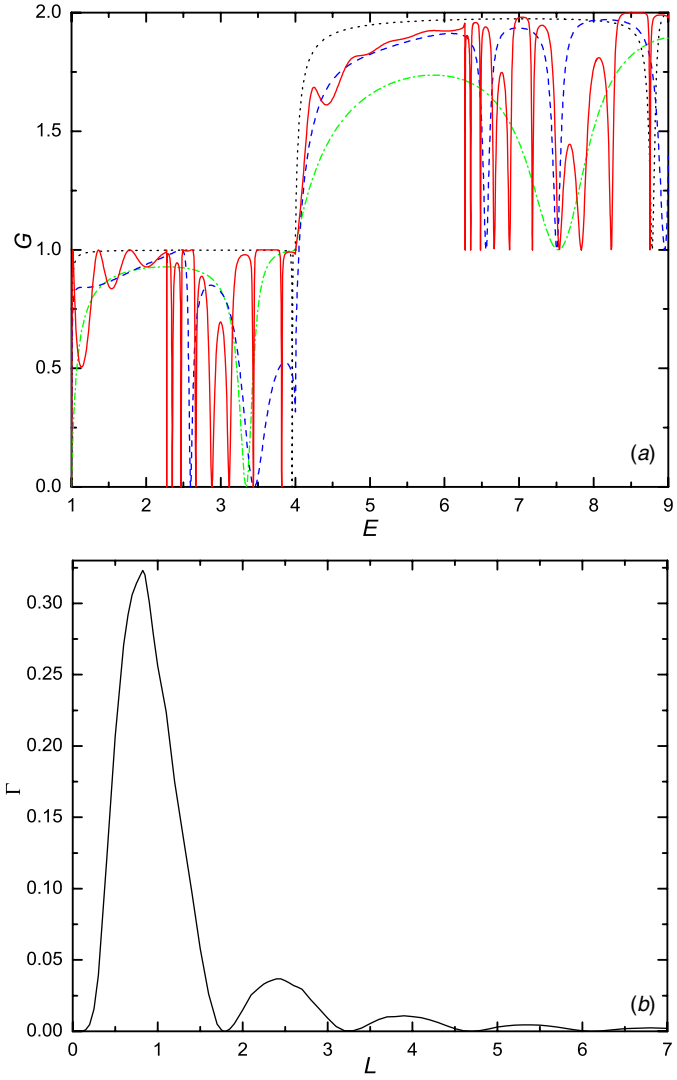

Figure 6. Field-free transport in the DD–DN–DD wave guide. (*a*) Conductance G as a function of energy E with $L = 0.2$ (dotted line), $L = 0.5$ (dash-dotted line), $L = 1.5$ (dashed line) and $L = 6$ (solid line). (*b*) Half-width Γ as a function of the length L.

With growing L, energy $E_{\min}$ decreases and at very large window lengths approaches asymptotically the value of $9/4$ which is the threshold boundary for the DN part. Half-width Γ is shown as a function of L in figure 6(*b*). It is seen that Γ increases with small and moderate values of the window length, reaches maximum, and then decreases to minimum of *zero* at $L = 1.791$ after which the whole situation is repeated again with smaller values of maximum Γ. Zero magnitude of the half-width in the minimum means, according to (30), that the corresponding level at this critical length turns into the true bound state with infinite lifetime. Energy E_{qb} in this case is a real value, as it follows from (31). As a result of the resonant interference phenomena in the DN junction, such a state does not decay since it does

not interact with its degenerate continuum counterpart. Accordingly, its wavefunction in the DD arms does not have a plane wave component, as it was the case for the quasi-bound level, exhibiting fading exponents only. True bound state degenerate with the continuum, or bound state in the continuum (BIC), appears as a very special solution of the wave equation. BICs were predicted to exist soon after the formulation of the quantum mechanics [54]. Summary of the research on the BICs up to the early 1980s is given in [55] and [56] where, however, a heavy emphasis is made on the mathematical side of the problem. BICs have been thoroughly discussed by the theoreticians from different branches of physics [8, 9, 11, 20, 26, 31, 57–72], and were detected experimentally in semiconductor superlattices [73–75] and crossed electromagnetic wave guides [76]. As we see, they also play an important role in determining transport properties of the channels with combined boundary conditions. Once again, we draw parallels with the curved DD [65] or DN [20] wave guide when, similar to considered here structure, BICs exist for some critical parameters of the bend only.

Figure 6(*a*) shows that with growing L other zero minima of the conductance G emerge with their total number increasing with L. For the very large window lengths they accumulate near 9/4, and their half-widths obey the same rules as the lowest quasi-bound state; in particular, for them BICs are also formed at some critical lengths L. Simultaneously, for the energies in the range $1 < E < 9/4$ Breit–Wigner-like resonances are formed with their maxima equal to unity. The number of these resonances increases with the window length. For the higher lying subbands, a picture of the conductance as a function of the energy E and length L remains basically the same. The only difference is the fact that, due to the interaction between the modes, corresponding maxima for the higher subbands are, in general, lower than the integer values. As is seen from figure 6(*a*), for large L the resonances in the second DD subband accumulate to the right of the energy $E = 25/4$ which is another DN propagation threshold.

The Neumann window on one of the walls destroys a transverse symmetry of the wave guide; namely, the upward motion in the DN section is not equivalent to the downward one. As a result, the BIC for this configuration emerges for the special window lengths only, as it was discussed above. It is known that the BICs reflect some symmetry of the system. In order to restore the transverse symmetry and, accordingly, to pave the way for the BICs existence at any L, one needs to introduce on the lower surface a second Neumann window of the same length what, in our notation, corresponds to the DD–NN–DD structure (figure 1(*b*)). It is easy to show that in this case the BICs exist for the arbitrary length L. Namely, in the semi-infinite leads for the fixed total energy E a longitudinal component of the energy E_x is $E_x|_{DD} = E - n^2$. For the same total energy E, in the NN junction between the leads, E_x takes the values $E_x|_{NN} = E - (l-1)^2, l = 1, 2, \ldots$. For bound state to exist, the longitudinal energy E_x should be positive in the NN junction and negative in the DD parts. Thus, total energy E should satisfy two inequalities simultaneously:

$$(l-1)^2 < E < n^2. \tag{32}$$

This condition corresponds to the propagation in the NN section and to the decay in the DD arms. The lowest solution of these inequalities $0 < E < 1$ is satisfied for $l = 1, n = 1$. In this case, we have a true bound state below the fundamental propagation threshold $E_{DD1}^{(TH)} = 1$ of the DD wave guide which was described above. Next, consider a situation with $l = 1, n = 2$ when the bound-state energy lies in the range $0 < E < 4$. If this energy, that is determined by L, is less than $E_{DD1}^{(TH)}$, then we have a second true bound level below the fundamental threshold. If, however, the energy is greater than 1, then the corresponding state is embedded into the continuum. Even though this BIC is degenerate with the propagating modes in the first DD subband, it does not interact with them since mentioned-above transverse symmetry

effectively decouples them. One gets the next BIC for $l = 2, n = 2$ when (32) transforms to $1 < E < 4$. Again, this level lies in the first propagation mode of the DD wave guide. In the same way, the BICs are obtained for the other permutations of the larger indices l and n. In particular, for $l = 1$ and growing n, we get next bound states below $E_{DD1}^{(TH)}$ if the general condition, equation (32), is strengthened by the requirement of the total energy being less than 1. For the energies larger than $E_{DD1}^{(TH)}$, one comes to the BICs lying in the fundamental as well as in the higher DD subbands. Thus, we see many analogies with the BIC for the straight Dirichlet strip with an embedded quantum dot [9, 31]. In both cases, the BICs are formed as a result of the level splittings from the higher lying mode either by the quantum dot or by the variation of the boundary conditions. For the transversely asymmetric quantum dot, the BICs emerge for some critical longitudinal dot dimensions only [9] which is also the case for the DN junction, as it was discussed above. At the same time, for the symmetric quantum dot [31], the BICs exist at arbitrary L. Similar to the quantum-dot case [31], a symmetry of our system and, accordingly, the BIC existence, can be destroyed by the applied magnetic field. We defer detailed discussion of this phenomenon to the following subsection.

3.2.2. Magnetotransport in the fundamental mode. Next, we discuss transport at nonzero fields. Figure 7(*a*) shows conductance G as a function of the energy E for the DD–DN–DD structure for several magnetic fields and $L = 1$. At $B = 0$ in this case, there are two zero minima of the conductance in the fundamental DD subband. An increasing magnetic field leads to the right shift of the energies $E_{\min}$ at which the minima are achieved. Conductance in the minimum $G_{\min}$, generally, ceases to be zero for non-vanishing magnetic fields. For example, for the minimum with larger $E_{\min}$ it monotonically increases with B, as figure 7(*b*) shows. At $B \simeq 6$, this minimum is completely dissolved. This means that at the higher fields the quasi-bound state ceases to exist. For comparison, in figure 7(*b*) we also plot $G_{\min}$ dependence on B for the same channel with $L = 0.2$ when only one minimum exists. At $B = 0$, its energy $E_{\min}|_{L=0.2} = 3.959$ is larger than the corresponding energy of the higher minimum when $L = 1$, $E_{\min}|_{L=1} = 3.899$. Despite this, this quasi-bound level survives stronger magnetic fields with its conductance in the minimum monotonically approaching unity with B growing. Explanation of the different behaviour of these two levels is similar to the case of the curved DD wave guide [44]. Namely, quasi-bound states in the first propagating mode are formed as a result of the interference mainly in the DN section. As a result, smaller fields with larger magnetic length $l_B = B^{-1/2}$ influence this interference for the wave guides with big enough L only. Quasi-bound states for the small L remain intact since for them a small magnetic field perturbs a particle motion mainly in the DD elbows. In other words, we can say that a total magnetic flux Φ through the DN junction

$$\Phi = BL \tag{33}$$

is proportional to its length and, accordingly, quasi-bound states are perturbed stronger by the field for larger L.

In contrast, compared to the previous two cases, the lower minimum of the wave guide with $L = 1$ is 'buried' much stronger into the DN junction. Accordingly, its minimum conductance is a nonmonotonic function of the magnetic field. In particular, rapid oscillations of $G_{\min}$ between zero and unity develop near $B \simeq 10$. For still higher magnetic fields, the magnitude of $G_{\min}$ again tends asymptotically to unity what means a dissolution of the corresponding quasi-bound state by the increasing magnetic field. Qualitatively, similar behaviour of the rapid oscillations of $G_{\min}$ with varying magnetic fields has been observed for the bent DD channel [44]. For the magnetic field, a definition of the half-width Γ should be modified to accommodate the case of nonzero $G_{\min}$; namely, now it is the difference between the energies

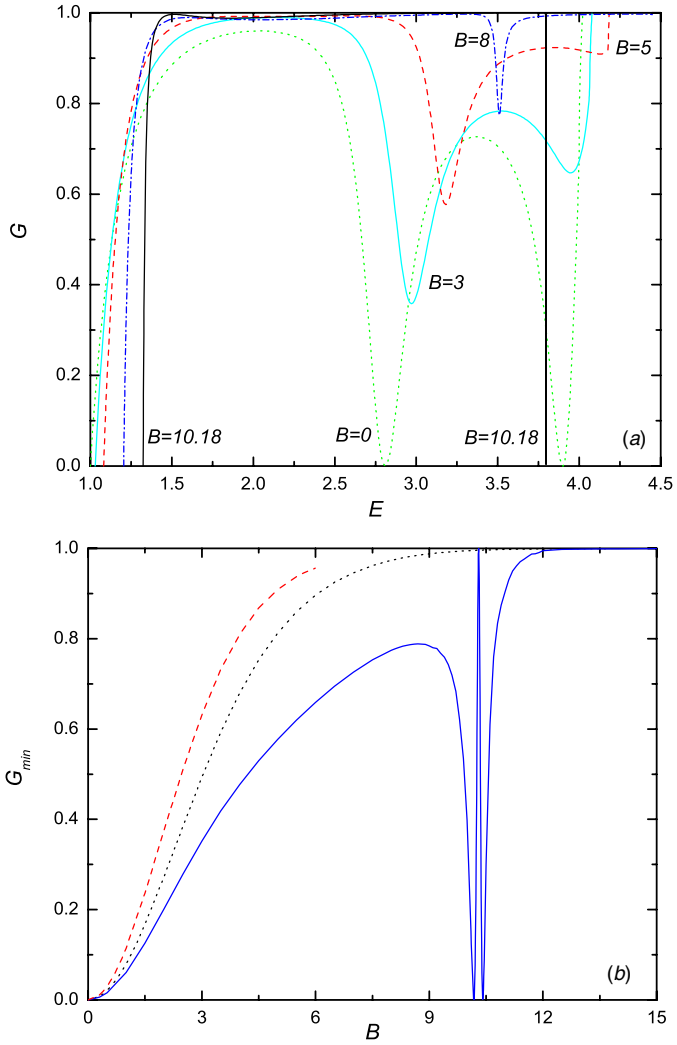

Figure 7. Magnetotransport in the DD–DN–DD wave guide. (*a*) Conductance G as a function of energy E with $L = 1$ and several magnetic fields. Numbers near the curves denote corresponding intensity B. (*b*) Conductance $G_{\min}$ corresponding to the minimum on G–E curve as a function of the field B for the higher (dashed curve) and lower (solid line) minima with the junction length $L = 1$ and for the minimum for $L = 0.2$ (dotted line).

at which the value of the conductance $G = (G_< + G_{\min})/2$ is achieved. We do not plot it here as a function of the field noting only that the half-width Γ diverges when the minimum conductance reaches unity. This means that the quasi-bound level has been completely wiped out by the magnetic field. Drawing again parallels with the curved DD wave guide [44], we see a qualitative similarity between these two cases when, changing parameters of the junction between two straight Dirichlet arms, one can vary $G_{\min}$ and Γ dependences on the magnetic fields.

Next, let us consider transport characteristics of the DD–NN–DD channel in the magnetic field. As we stated above, in the absence of the fields the BICs exist for this strip at any junction length L. The BIC does not interact with its degenerate continuum counterpart since

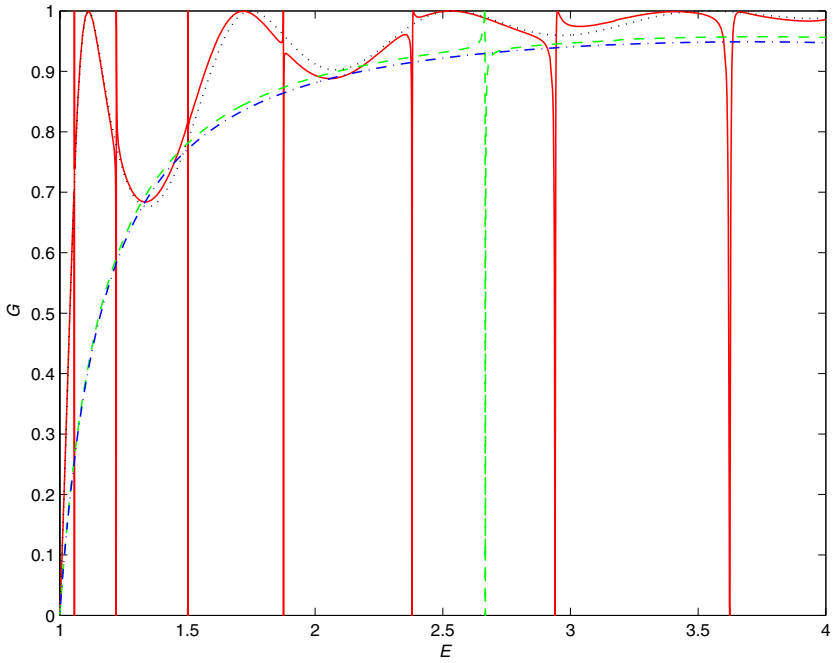

Figure 8. Conductance of the DD–NN–DD wave guide for $L = 0.5$ and $B = 0$ (dash-dotted line), $L = 0.5$ and $B = 0.3$ (dashed line), $L = 4$ and $B = 0$ (dotted line), $L = 4$ and $B = 0.3$ (solid line).

they are effectively decoupled due to their different symmetries. Applied magnetic field mixes transverse and longitudinal motions in the wave guide thus destroying the symmetry of the system. As a result, the BICs cease to exist upon application of the magnetic field transforming instead into the resonances which are quasi-bound states with finite lifetime. This is vividly manifested in figure 8 which shows conductances of the DD–NN–DD channel with $L = 0.5$ and $L = 4$ for zero and nonvanishing magnetic field. It is seen that the small magnetic field leads to the transformation of the smooth conductance-energy dependence into the curve with one or several regions of the abrupt G variation between zero and unity. These are ubiquitous Fano resonances [13, 77] which also appear, for example, when the BIC in the quasi-one-dimensional wave guide with symmetrical scatterer is destroyed by the applied magnetic field [31], the bend [66] or shift from the centre line [7]. In all cases, the resonances grow narrower with decreasing the relative strength of the symmetry-breaking perturbation, until they become the BICs when this perturbation vanishes. Thus, location of these resonances on the E axis allows one to determine the BIC energy. A number of the BICs increase with the junction length which is also the case for the bound states below the fundamental DD threshold, as was discussed above. For example, for $L = 0.5$, we observe one Fano resonance, and for $L = 4$ this number increases to 7. Note that similar to the DD wave guide with a symmetrically embedded quantum dot [31], for the different Fano resonances in figure 8, a mutual location on the energy axis of their minima and maxima with respect to each other can be different too. This corresponds to a positive (minimum precedes maximum) or negative (maximum before minimum) asymmetry parameter q in the Fano formula [13, 77]

$$f(\varepsilon) = \frac{(\varepsilon + q)^2}{\varepsilon^2 + 1}. \tag{34}$$

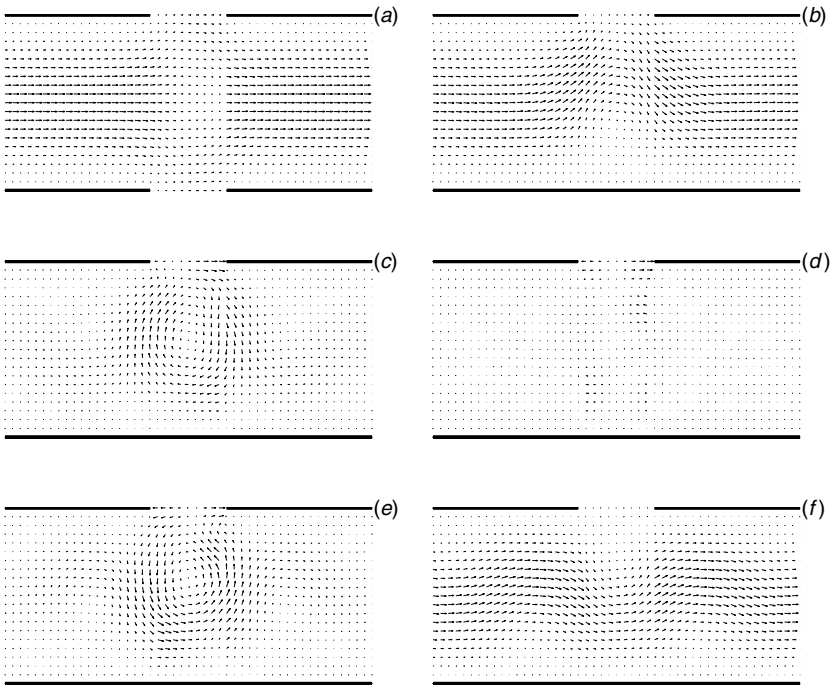

Figure 9. Current densities of the DD–NN–DD (panel (*a*)) and DD–DN–DD (panels (*b*)–(*f*)) wave guides with $L = 0.5$ at zero magnetic field and energies: (*a*) $E = 2.5$ (conductance $G = 0.922$), (*b*) $E = 2.8$ ($G = 0.881$), (*c*) $E = 3.27$ ($G = 0.260$), (*d*) $E = 3.35$ ($G = 0.009$), (*e*) $E = 3.4$ ($G = 0.254$), (*f*) $E = 3.95$ ($G = 0.996$). Thick horizontal lines denote the Dirichlet walls of the wave guide, and the gaps between them symbolize Neumann boundary conditions. Larger arrows denote higher currents. For each of the figures the currents are normalized with respect to their largest value.

Here $\varepsilon = (E - E_R)/(\Gamma/2)$ is the dimensionless energy in units of the resonance width Γ and E_R is the resonance energy of the Fano transition.

3.3. Current density patterns

To get a deeper insight into the transport properties, it is instructive to investigate currents flowing in the wave guide. Current density in the magnetic field is given as [15, 48]

$$\mathbf{j} = -\mathrm{Im}[\Psi^*(\mathbf{r})\nabla\Psi(\mathbf{r})] - \mathbf{A}\Psi^*(\mathbf{r})\Psi(\mathbf{r}). \tag{35}$$

Before discussing currents in the magnetic fields, we briefly analyse the situation at $B = 0$. Figure 9 shows current densities at different energies E for the DD wave guide with the NN and DN junctions with $L = 0.5$. Corresponding G–E dependences are shown by the dash-dotted lines, respectively, in figures 8 and 6(*a*). For the NN junction, when the conductance is a smooth function of the Fermi energy, the current preserves the laminar flow at any energy. An example of such distribution is shown in figure 9(*a*) for $E = 2.5$ that is close to the BIC energy. Similar current distributions are observed for the other energies as well. However, a situation is very different for the DN junction when, instead of the BIC, a quasi-bound state exists between the two Dirichlet leads. According to our discussion in section 3.2, it causes the conductance to drop abruptly to zero. As figure 9 shows, it also induces current vortices. Namely, when the energy is far away from $E_{\min}$, one observes a laminar charge flow in the

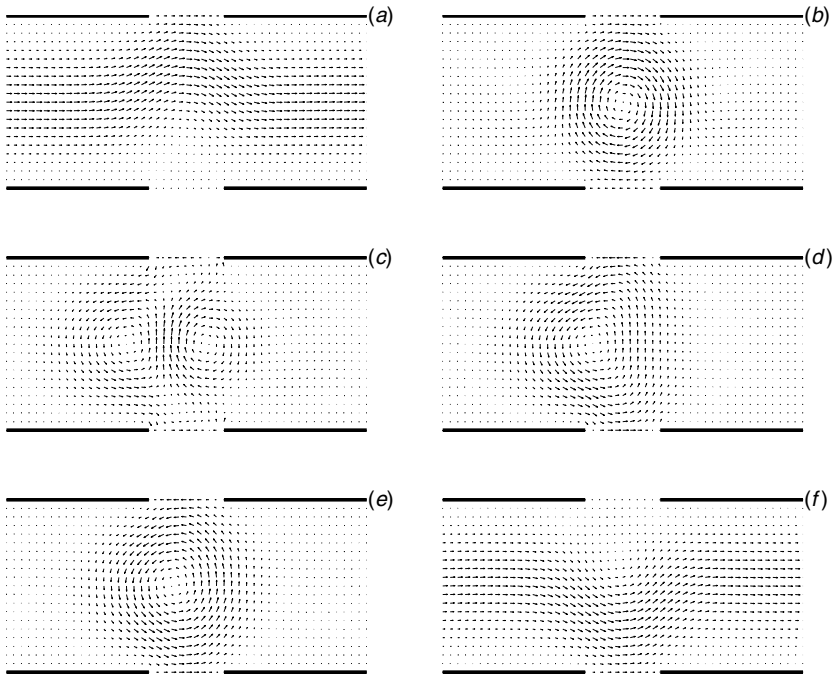

Figure 10. Current densities of the DD–NN–DD channel with $L = 0.5$ at $B = 0.3$ and energies (*a*) $E = 2.62$ (conductance $G = 0.942$), (*b*) $E = 2.664$ ($G = 1$), (*c*) $E = 2.666$ ($G = 0.638$), (*d*) $E = 2.666\,65$ ($G = 0$), (*e*) $E = 2.668$ ($G = 0.644$), (*f*) $E = 2.7$ ($G = 0.929$). All other agreements are the same as in figure 9.

leads with a smooth transition to the current in the DN part which is mainly localized near the Neumann wall. When the energy E moves closer to $E_{\min}$, a vortex starts to develop in the junction. One of the initial stages of the formation of the vortex is depicted in figure 9(*b*). Far away in the Dirichlet arms, the current still has a longitudinal component only. Further slight increase of the energy transforms the current in the junction and its closest neighbourhood into the closed vortex (figure 9(*c*)). A number of the vortices increase with the junction length. Similar to the other configurations [6, 20, 21, 34, 66, 78–80], seeding of the vortices into the current density is a result of the strong intersubband interaction which adds a transverse component to the particle flow. In a particular case of the DD–DN–DD wave guide, a strength of the vortex varies with energy E; for example, as one continues to approach $E_{\min}$ from the left, the vortex gradually dissolves, and at very small conductances it completely disappears (figure 9(*d*)). It emerges again for $E > E_{\min}$; however, the vortex rotation has changed its azimuthal direction, as the comparison of panels (c) and (e) shows. Earlier, the change of the vortex direction after passing the conductance extremum has been predicted to occur for the DD wave guide with the impurity or the bend [20, 66, 78]. However, for the straight channel with the DN part, a switch of the vorticity sign is a gradual process in contrast to the abrupt chirality reversal at the energy of the reflection resonance, say, for the curved wave guide [78]. When the energy increases further, the vortex dissolves with the closed loop of the flow broken at the Neumann wall, as is shown in figure 9(*f*). A comparative analysis of panels (*f*) and (*b*) leads to the same conclusions as the discussion of figures 9(*e*) and 9(*c*).

As a representative example of the magnetic field influence on the currents in the wave guide with mixed boundary conditions, we show in figure 10 current densities corresponding to the DD–NN–DD channel with $L = 0.5$ in the magnetic field $B = 0.3$ and several energies

E (dashed line in figure 8). Similar to the previous cases, a gradual formation of the vortex is seen as one comes closer to the resonance (panel (a)). After passing the Fano maximum (panel (b)), in the energy region between the two extrema, the circular vortex shifts to the left simultaneously gradually dividing into two rotations with the opposite angular directions (panel (c)). One of the vortices gradually fades away and, thus, in the minimum of the conductance (panel (d)) and to the right of it (panel (e)) we observe again one vortex only with its chirality, however, being opposite to the one in the maximum or in the region to the left of it. As one can see, a change of the azimuthal vortex rotation in this case is different from the field-free channel with the DN junction, curved wave guide [20, 66, 78] or straight Dirichlet strip with a quantum dot in the magnetic field [31]. Far away to the right, the vortex gradually dissolves with the loop broken first at the upper wall. In fact, panel (f) can be obtained from figure 10(a) via the mirror reflection with respect to the plane $y = 0$. Semiclassically, the formation of the vortices corresponds to the bounded motion in the junction. A particle traversing the structure enters the scattering area, dwells there during the time τ determined by the half-width Γ, equation (30), and subsequently leaves it in one or other longitudinal direction. We want to emphasize that the vortices in considered structures are a result of the geometry-induced interference between the different subbands. Accordingly, they are different from the circular motion of Cooper pairs in superconductors [15]. In particular, as pointed out earlier for the similar case [31], each of the vortices does not carry the flux quantum. As we have shown in figure 9, the vortices, for the special geometries, develop even in the absence of the fields. Each of them presents a localized magnetic moment and, therefore, eventually, can be detected in the experiments.

4. Concluding remarks

We have considered theoretically the properties of the straight wave guide with combined Dirichlet and Neumann boundary conditions. It was predicted that bound states in the continuum exist both for the DD–DN–DD and DD–NN–DD strips. However, for the former case it takes place for some critical window lengths only, and for the two symmetrically embedded Neumann segments on the opposite sides of the wave guide, it is true for their arbitrary lateral extent. Applied magnetic fields couple the BIC with its degenerate continuum counterpart thus transforming it into a quasi-bound state with finite lifetime what, for the symmetric configuration, leads to the appearance of the Fano resonances on the conductance-energy dependence. Growing magnetic fields also induce new bound states lying below the fundamental propagation threshold of the Dirichlet arms.

Above, we considered a situation with the DD semi-infinite arms and the DN or NN junction. There is no any difficulty for extending the results to other configurations of the boundary conditions. For example, for the NN–DD–NN structure equation (32) for the BIC existence is transformed as

$$n^2 < E < (l-1)^2. \tag{36}$$

It shows that in this case BICs do not exist in the fundamental propagation subband of the NN strip, $0 < E < 1$, emerging for the higher lying modes only. Analysis of the influence of the magnetic fields on this and other similar structures, for example, those discussed in [17], can be performed in the same way as was done above.

Next, we discuss the possible experimental verification of our theoretical consideration. Throughout the whole paper we kept our results applicable both to the semiconductors as well as superconductors. The most obvious candidate for the experimental test is the superconducting nanometer-width strip flanked by the different non-superconducting

substrates. Modern technology allows one to assemble nanodevices where aluminum-based superconductor electrodes are attached to the individual InAs semiconductor nanowires [81] or carbon nanotubes [82]. By varying the gate voltage, the conductance in such structures can be tuned from the superconductor behaviour to the normal-state currents. From the phenomenological Landau–Ginsburg theory for superconductors it is well known that the order parameter, $\Psi(\mathbf{r})$ which satisfies (3) with $q = 2e$ and M being double electronic mass, obeys the following boundary condition [15] (we return here to the dimensional units):

$$\frac{1}{\Psi}\left(\nabla\Psi + i\frac{2e}{\hbar}\mathbf{A}\Psi\right)\mathbf{n} = \frac{1}{b}. \tag{37}$$

The value of $1/b$ can be safely put to zero for the insulator or the vacuum since in this case $b \sim 1$ cm which is enormous at the relevant scale [15]. However, for the boundary with the non-superconducting metals $1/b$ ceases to be zero and can take large values [15], especially for the magnetic materials. Moreover, as was theoretically shown recently, when a strong electric field $\boldsymbol{\mathcal{E}}$ is applied to the interface, the right-hand side of (37) should be supplemented (for zero magnetic field) by the term $\mathcal{E}/U_s$, where the effective potential U_s is expressed via the usual parameters of the Landau–Ginsburg theory [83]. Thus, choosing relevant materials and applying appropriate temperatures and magnetic and electric fields, one can come to the regime described in the present paper. In fact, varying the parameter $1/b$, one can change mixed boundary conditions at will. Quantum structures with different 'mixing' parameter $1/b$ were theoretically discussed in mesoscopic physics [84, 85]. Calculations of the straight wave guide with such boundary conditions in the uniform magnetic fields are now in progress.

Appendix

Scattering $\mathbf{S}(E)$ and reflection $\mathbf{R}(E)$ matrices of the straight DD–DN–DD wave guide in uniform magnetic field are given as

$$\mathbf{S} = \mathbf{P}_+\mathbf{L}(\mathbf{I} - \mathbf{P}_-^T\mathbf{P}_-)^{-1}\mathbf{P}_+^T \tag{A.1a}$$

$$\mathbf{R} = \mathbf{P}_-(\mathbf{I} - \mathbf{P}_-^T\mathbf{P}_-)^{-1}\mathbf{P}_+^T, \tag{A.1b}$$

where $\mathbf{I}$ is the infinite identity matrix, superscript T denotes a transposed matrix, and infinite matrices $\mathbf{P}_\pm$ and $\mathbf{L}$ have the following elements:

$$(\mathbf{P}_\pm)_{nn'} = \int_{-1/2}^{1/2}\left[\pm p_n^{(DD)} + p_{n'}^{(DN)} - 2By\right]\chi_{\pm p_n}^{(DD)}(y)\chi_{p_{n'}}^{(DN)}(y)\,\mathrm{d}y \tag{A.2a}$$

$$\mathbf{L}_{nn'} = \exp\left(\mathrm{i}p_n^{(DN)}L/2\right)\delta_{nn'}. \tag{A.2b}$$

Bound-state energies are determined from the following equation:

$$\det\left\|\left(\mathbf{I} - \mathbf{P}_+^T\mathbf{P}_+\right)\mathbf{L} + (\mathbf{I} - \mathbf{P}_-^T\mathbf{P}_-)\mathbf{L}^{-1}\right\| = 0. \tag{A.3}$$

Clear analogy with the curved DD wave guide [44] is seen. Since in the literature [86, 87] there are no explicit expressions for the integrals in the matrices $\mathbf{P}_\pm$, their direct numerical quadrature was performed.

References

[1] van Wees B J, van Houten H, Beenakker C W J, Williamson J G, Kouwenhoven L P, van der Marel D and Foxon C T 1988 *Phys. Rev. Lett.* **60** 848

[2] Wharam D A, Thornton T J, Newbury R, Pepper M, Ahmed H, Frost J E F, Hasko D G, Peacock D C, Ritchie D A and Jones G A C 1988 *J. Phys. C: Solid State Phys.* **21** L209
[3] Chu C S and Sorbello R S 1989 *Phys. Rev.* B **40** 5941
[4] Bagwell P F 1990 *Phys. Rev.* B **41** 10354
Bagwell P F 1990 *J. Phys.: Condens. Matter* **2** 6179
[5] Tekman E and Ciraci S 1990 *Phys. Rev.* B **42** 9098
[6] Chaudhuri S, Bandyopadhyay S and Cahay M 1992 *Phys. Rev.* B **45** 11126
[7] Tekman E and Bagwell P F 1993 *Phys. Rev.* B **48** 2553
[8] Exner P, Gawlista R, Šeba P and Tater M 1996 *Ann. Phys., NY* **252** 133
[9] Kim C S, Satanin A M, Joe Y S and Cosby R M 1999 *Phys. Rev.* B **60** 10962
[10] Vargiamidis V and Polatoglou H M 2005 *Phys. Rev.* B **71** 075301
[11] Exner P and Němcová K 2002 *J. Math. Phys.* **43** 1152
[12] Bardarson J H, Magnusdottir I, Gudmundsdottir G, Tang C-S, Manolescu A and Gudmundsson V 2004 *Phys. Rev.* B **70** 245308
[13] Fano U 1961 *Phys. Rev.* **124** 1866
[14] Faist J, Guéret P and Rothuizen H 1990 *Phys. Rev.* B **42** 3217
[15] de Gennes P G 1966 *Superconductivity of Metals and Alloys* (New York: Benjamin)
[16] Bulla W, Gesztesy F, Renger W and Simon B 1997 *Proc. Am. Math. Soc.* **125** 1487
[17] Dittrich J and Kříž J 2002 *J. Math. Phys.* **43** 3892
[18] Dittrich J and Kříž J 2002 *J. Phys. A: Math. Gen.* **35** L269
Krejčiřík D and Kříž J 2005 *Publ. Res. Inst. Math. Sci.* **41** 757
Johnson E R, Levitin M and Parnovski L 2006 *SIAM J. Math. Anal.* **37** 1465
[19] Borisov D, Exner P and Gadyl'shin R 2002 *J. Math. Phys.* **43** 6265
Borisov D and Exner P 2004 *J. Phys. A: Math. Gen.* **37** 3411
[20] Olendski O and Mikhailovska L 2003 *Phys. Rev.* E **67** 056625
[21] Exner P, Šeba P, Tater M and Vaněk D 1996 *J. Math. Phys.* **37** 4867
[22] Frolov S V and Popov I Y 2000 *J. Math. Phys.* **41** 4391
[23] Kunze C 1993 *Phys. Rev.* B **48** 14338
[24] Larkin I A and Sukhorukov E V 1994 *Phys. Rev.* B **49** 5498
[25] Exner P and Vugalter S A 1996 *Ann. Inst. Henri Poincaré* A **65** 109
[26] Linton C M and Ratcliffe K 2004 *J. Math. Phys.* **45** 1359
[27] Maglione E, Ferreira L S and Cattapan G 2006 *J. Phys. A: Math. Gen.* **39** 1207
[28] Chakraborty T and Pietiläinen P 1995 *The Quantum Hall Effects : Integral and Fractional* (Berlin: Springer)
[29] Streda P, Kucera J and MacDonald A H 1987 *Phys. Rev. Lett.* **59** 1973
[30] Lee Y, McLennan M J and Datta S 1991 *Phys. Rev.* B **43** 14333
[31] Nöckel J U 1992 *Phys. Rev.* B **46** 15348
[32] Chaudhuri S, Bandyopadhyay S and Cahay M 1993 *Phys. Rev.* B **47** 12649
[33] Palacios J J and Tejedor C 1993 *Phys. Rev.* B **48** 5386
[34] Marigliano Ramaglia V, Ventriglia F and Zucchelli G P 1993 *Phys. Rev.* B **48** 2445
[35] Akis R, Vasilopoulos P and Debray P 1997 *Phys. Rev.* B **56** 9594
[36] Amemiya K 1999 *J. Phys. Soc. Japan* **68** 567
Amemiya K 2003 *J. Phys. Soc. Japan* **72** 135
[37] Gudmundsson V, Lin Y-Y, Tang C-S, Moldoveanu V, Bardarson J H and Manolescu A 2005 *Phys. Rev.* B **71** 235302
[38] Kirczenow G, Sachrajda A S, Feng Y, Taylor R P, Henning L, Wang J, Zawadzki P and Coleridge P T 1994 *Phys. Rev. Lett.* **72** 2069
Gould C, Sachrajda A S, Feng Y, Delage A, Kelly P J, Leung K and Coleridge P T 1995 *Phys. Rev.* B **51** 11213
Gould C, Sachrajda A S, Dharma-wardana M W C, Feng Y and Coleridge P T 1996 *Phys. Rev. Lett.* **77** 5272
[39] Borisov D, Ekholm T and Kovařík H 2005 *Ann. Henri Poincaré* **6** 327
[40] Hirayama Y, Wieck A D, Bever T, von Klitzing K and Ploog K 1992 *Phys. Rev.* B **46** 4035
Hirayama Y, Tokura Y, Wieck A D, Koch S, Haug R J, von Klitzing K and Ploog K 1993 *Phys. Rev.* B **48** 7991
[41] Smith C G 1996 *Rep. Prog. Phys.* **59** 235
[42] Luttinger J M and Kohn W 1955 *Phys. Rev.* **97** 869
[43] Schult R L, Wyld H W and Ravenhall D G 1990 *Phys. Rev.* B **41** 12760
[44] Olendski O and Mikhailovska L 2005 *Phys. Rev.* B **72** 235314
[45] Miller J C P 1955 *Tables of Weber Parabolic Cylinder Functions* (London: Her Majesty's Stationery Office)
Kireeva I E and Karpov K A 1961 *Tables of Weber Functions* (Oxford: Pergamon)
[46] Kraut E A 1967 *Fundamentals of Mathematical Physics* (New York: McGraw-Hill)

[47] Landauer R 1957 *IBM J. Res. Dev.* **1** 223
[48] Landau L D and Lifshitz E M 1977 *Quantum Mechanics (Non-Relativistic Theory)* (New York: Pergamon)
[49] Weidl T 1999 *Commun. Partial Differ. Equ.* **24** 25
[50] Balinsky A, Laptev A and Sobolev A V 2004 *J. Stat. Phys.* **116** 507
[51] Melgaard M, Ouhabaz E-M and Rozenblum G 2004 *Ann. Henri Poincaré* **5** 979
[52] Pippard A B 1983 *The Physics of Vibration* part 2 (Cambridge: Cambridge University Press)
[53] Ekholm T and Kovařík H 2005 *Commun. Partial Differ. Equ.* **30** 539
[54] von Neumann J and Wigner E 1929 *Phys. Zeit.* **30** 465
[55] Albeverio S 1972 *Ann. Phys., NY* **71** 167
[56] Eastham M S P and Kalf H 1982 *Schrödinger-type Operators with Continuous Spectra* (Boston: Pitman)
[57] Stillinger F H and Herrick D R 1975 *Phys. Rev.* A **11** 446
[58] Friedrich H and Wintgen D 1985 *Phys. Rev.* A **31** 3964
Friedrich H and Wintgen D 1985 *Phys. Rev.* A **32** 3231
[59] Robnik M 1986 *J. Phys. A: Math. Gen.* **19** 3845
[60] Schult R L, Ravenhall D G and Wyld H W 1989 *Phys. Rev.* B **39** 5476
[61] Evans D V, Levitin M and Vassiliev D 1994 *J. Fluid Mech.* **261** 21
[62] Stahlhofen A A 1996 *J. Phys. A: Math. Gen.* **29** L581
[63] Khelashvili A and Kiknadze N 1996 *J. Phys. A: Math. Gen.* **29** 3209
[64] Petrović J S, Milanović V and Ikonić Z 2002 *Phys. Lett.* A **300** 595
[65] Olendski O and Mikhailovska L 2002 *Phys. Rev.* B **66** 035331
[66] Olendski O and Mikhailovska L 2003 *Phys. Rev.* B **67** 035310
[67] Cederbaum L S, Friedman R S, Ryaboy V M and Moiseyev N 2003 *Phys. Rev. Lett.* **90** 013001
[68] Ladrón de Guevara M L, Claro F and Orellana P A 2003 *Phys. Rev.* B **67** 195335
Ladrón de Guevara M L and Orellana P A 2006 *Phys. Rev.* B **73** 205303
[69] Ordonez G and Kim S 2004 *Phys. Rev.* A **70** 032702
Ordonez G, Na K and Kim S 2006 *Phys. Rev.* A **73** 022113
[70] Sadreev A F, Bulgakov E N and Rotter I 2006 *Phys. Rev.* B **73** 235342
[71] Orrigo S E A, Lenske H, Cappuzzello F, Cunsolo A, Foti A, Lazzaro A, Nociforo C and Winfield J S 2006 *Phys. Lett.* B **633** 469
[72] Voo K-K and Chu C S 2006 *Phys. Rev.* B **74** 155306
[73] Sirtori C, Capasso F, Faist J, Sivco D L, Chu S-N G and Cho A Y 1992 *Appl. Phys. Lett.* **61** 898
Capasso F, Sirtori C, Faist J, Sivco D L, Chu S-N G and Cho A Y 1992 *Nature* **358** 565
[74] Sung B, Chui H C, Martinet E L and Harris J S Jr 1996 *Appl. Phys. Lett.* **68** 2720
[75] Vladimirova M R, Kavokin A V, Kaliteevskiĭ M A, Kokhanovskiĭ S I, Sasin M É and Seĭsyan R P 1999 *Pis'ma Zh. Eksp. Teor. Fiz.* **69** 727 (in Russian)
Vladimirova M R, Kavokin A V, Kaliteevskiĭ M A, Kokhanovskiĭ S I, Sasin M É and Seĭsyan R P 1999 *JETP Lett.* **69** 779 (Engl. Transl.)
[76] Annino G, Yashiro H, Cassettari M and Martinelli M 2006 *Phys. Rev.* B **73** 125308
[77] Connerade J-P and Lane A M 1988 *Rep. Prog. Phys.* **51** 1439
[78] Šimánek E 1999 *Phys. Rev.* B **59** 10152
[79] Bromley M W J and Esry B D 2004 *Phys. Rev.* A **70** 013605
[80] Laux S E, Kumar A and Fischetti M V 2004 *J. Appl. Phys.* **95** 5545
[81] Doh Y-J, van Dam J A, Roest A L, Bakkers E P A M, Kouwenhoven L P and De Franceschi S 2005 *Science* **309** 272
[82] Jarillo-Herrero P, van Dam J A and Kouwenhoven L P 2006 *Nature* **439** 953
[83] Lipavský P, Morawetz K, Koláček J and Yang T J 2006 *Phys. Rev.* B **73** 052505
[84] Hornberger K and Smilansky U 2001 *J. Phys. A: Math. Gen.* **33** 2829
Hornberger K and Smilansky U 2002 *Phys. Rep.* **367** 249
[85] Baelus B J, Partoens B and Peeters F M 2006 *Phys. Rev.* B **73** 212503
[86] Gradshteyn I S and Ryzhik I M 2000 *Table of Integrals, Series, and Products* (New York: Academic)
[87] Prudnikov A P, Brychkov Yu A and Marichev O I 1986 *Integrals and Series* vol 2 (New York: Gordon and Breach)